MODELING WAVE DAMPING AND SEDIMENT TRANSPORT WITHIN A PATCH OF VEGETATION

Gangfeng Ma[1]

Vegetation canopies control mean and turbulent flow structures as well as suspended sediment processes in the coastal wetlands. In this study, a three-dimensional hydrodynamic and sediment transport model is developed for studying flow/wave-vegetation-sediment interactions. The model is based on the non-hydrostatic model NHWAVE. The vegetation effects on turbulent flow are accounted for by introducing additional formulations associated with vegetation-induced drag and turbulence production in the governing equations. The sediment concentration is obtained by solving the advection-diffusion equation with sediment exchange at the bed. The turbulent flow and suspended sediment are simulated in a coupled manner. The model is validated against the laboratory measurements of partially vegetated open channel flows. It is shown that the model can well predict the vegetation effects on the flow field. The model is then employed to study nearshore sediment suspension influenced by a patch of vegetation, which is located in the surf zone. The turbulence generated by wave breaking is greatly damped by the vegetation patch, resulting in considerably less sediment pickup from the bottom in the surf zone. Within the vegetation patch, most suspended sediments are restricted in a thin layer near the bottom. The net sediment transport is in the shoreward direction, in contrast to the seaward net transport of sediments in the unvegetated surf zone.

Keywords: NHWAVE, vegetated flow, sediment transport, nearshore sediment flux

INTRODUCTION

Aquatic vegetation play a significant role in controlling mean flow, turbulence as well as sediment processes. Due to the enhanced resistance associated with the plants, the mean flow is greatly reduced within the vegetation patch, compressing turbulence level (Nepf, 1999) and promoting sedimentation and the retention of suspended sediments (Lopez and Garcia, 1998; Sharp and James, 2006; Zong and Nepf, 2010). The resulting spatial depositional patterns are the key to the understanding of the long-term morphologic and ecological dynamics of tidal marshes and floodplains (Temmerman et al., 2005). In the coastal wetlands, sediment deposition determines the ability of tidal marshes to keep pace with the accelerated sea level rise.

Up to date, most of our knowledge on sediment transport processes and sedimentation within vegetation patches comes from the laboratory flume studies. For example, Abt et al. (1995) and Thornton et al. (1997) performed a series of laboratory experiments to assess the deposition and entrapment in riparian vegetation. Their results showed that the presence of the vegetation not only increases the deposition of sediment, but also the entrapment of sediment on the vegetative bases. It was determined that vegetation could retain 30 to 70 percent of the deposited sediments. They also found that the length and cross-sectional area of the vegetation are two dominant factors in controlling the ability of vegetation to entrap and retain sediments. Garcia et al. (1999) studied the effect of seagrass on the flow and sediment entrapment by conducting a series of experiments with the presence and absence of the seagrass. They showed that there is a direct relationship between the height of the plants and reduction of flow velocity. The amount of the particles trapped by seagrass is closely related to the surface area of the plants. Elliot (2000) investigated the removal of sediment in a channel by means of settling on the vegetation. It was theoretically and experimentally shown that the settling on vegetation can considerably enhance the sediment capture process. Sharpe and James (2005) performed a series of laboratory experiments to study how emergent vegetation promotes sediment deposition. They found that the suspended transport and the extent of longitudinal deposits from suspension within emergent stems is enhanced by increased flow depth and reduced by increased sediment grain size and stem density. Zong and Nepf (2010, 2011) conducted laboratory experiments to investigate flow and sediment deposition in and around a finite patch of vegetation in an open channel. Their studies revealed the existence of a diverging flow at the leading edge of the vegetation patch and a shear layer with large-scale coherent vortices at the lateral interface between the patch and adjacent open channel, which have significant effects on sediment deposition within the patch.

Although the flume studies have enlarged our insights on vegetated flow and associated sediment processes, the flow-vegetation-sediment interactions on the landscape scale (i.e. length scale of 10^2 - 10^3 m) are still poorly understood because field monitoring of three-dimensional flow field and sediment deposition within vegetation patches is extremely difficult. In this respect, numerical modeling may provide a

[1]Department of Civil and Environmental Engineering, Old Dominion University, USA

powerful tool for investigating these complicated interactions in the field-scale. The traditional approach for modeling flow and sediment transport in vegetation canopy is to solve the depth-averaged shallow-water equations and to use an enhanced bottom roughness coefficient (i.e. Manning coefficient) for vegetated surfaces, for instance, Wu et al. (2005), Chen et al. (2007). Such an approach, however, does not account for the influence of vegetation over the entire water depth (Temmerman et al., 2005), thus is not able to accurately capture three-dimensional flow-vegetation interactions and associated suspended sediment processes. A more sophisticated approach is to solve the hydrodynamic and sediment transport equations by including additional formulations for drag and turbulence production induced by vegetation canopies. For example, Lopez and Garcia (1998) developed a 1DV model to study sediment suspension in the vegetated open channel. Their model accounted for vegetation effects by introducing drag terms in the momentum equations and additional turbulence production in $k-\epsilon$ equations. Temmerman et al. (2005) developed a three-dimensional vegetated flow and sediment transport model based on Delft3D. The strategy in their model was similar to that of Lopez and Garcia (1998). The model was applied to investigate the impact of vegetation on flow routing and sedimentation patterns in a field-scale tidal marsh. Sheng et al. (2012) developed a similar vegetated flow model based on CH3D and applied it to study the reduction of storm surge by vegetation canopies. These models are hydrostatic, and not capable of simulating wave-vegetation interactions.

In this paper, we aim to develop a 3D hydrodynamic and sediment transport model that is capable of simulating flow/wave-vegetation-sediment interactions. The model is based on the Non-Hydrostatic WAVE model NHWAVE, which was initially developed by Ma et al. (2012). The vegetation-induced turbulence production is simulated by a nonlinear $k-\epsilon$ turbulence model. The sediment concentration is obtained by solving the advection-diffusion equation with sediment exchange at the bed. The model is validated against the laboratory measurements of Pasche and Rouve (1985). Then the model is applied to study nearshore sediment suspension affected by a finite patch of vegetation.

The remainder of the paper is organized as follows. The mathematical models including the non-hydrostatic model NHWAVE, the nonlinear $k-\epsilon$ turbulence closure and sediment transport model are introduced in section 2. The nearshore sediment suspension and cross-shore sediment fluxes are also discussed in section 3. The conclusions are finally given in section 4.

MATHEMATICAL MODELS

Governing Equations

Ma et al. (2013a) have developed a 3D vegetated flow model that is capable of simulating wave damping induced by vegetation canopy. The model was based on the Non-Hydrostatic WAVE model NHWAVE, which was initially developed by Ma et al. (2012) and extensively used to study landslide-induced tsunami waves (Ma et al., 2013b), infragravity wave process in coral reef systems (Ma et al., 2014a) and wave interactions with porous structures (Ma et al., 2014b). NHWAVE solves the incompressible Reynolds Averaged Navier-Stokes equations in well-balanced conservative form, formulated in time-dependent surface and terrain-following σ coordinate. The model employs an arbitrary stretched vertical grid, which is able to accurately resolve bottom boundary layer and sediment suspension processes. The terrain-following σ-coordinate is defined as

$$t = t^* \quad x = x^* \quad y = y^* \quad \sigma = \frac{z^* + h}{D}$$

where $D(x, y, t) = h(x, y) + \eta(x, y, t)$, h is water depth, η is surface elevation.

With σ coordinate transformation, the well-balanced mass and momentum conservation equations are given by

$$\frac{\partial D}{\partial t} + \frac{\partial Du}{\partial x} + \frac{\partial Dv}{\partial y} + \frac{\partial \omega}{\partial \sigma} = 0 \tag{1}$$

$$\frac{\partial \mathbf{U}}{\partial t} + \frac{\partial \mathbf{F}}{\partial x} + \frac{\partial \mathbf{G}}{\partial y} + \frac{\partial \mathbf{H}}{\partial \sigma} = \mathbf{S}_h + \mathbf{S}_p + \mathbf{S}_\tau + \mathbf{S}_\rho + \mathbf{S}_v \tag{2}$$

where $\mathbf{U} = (Du, Dv, Dw)^T$. (u, v, w) are velocity components in (x, y, z) directions. ω is the vertical velocity in σ coordinate. The fluxes in the momentum equations are

$$\mathbf{F} = \begin{pmatrix} Duu + \frac{1}{2}g\eta^2 + gh\eta \\ Duv \\ Duw \end{pmatrix} \quad \mathbf{G} = \begin{pmatrix} Duv \\ Dvv + \frac{1}{2}g\eta^2 + gh\eta \\ Dvw \end{pmatrix} \quad \mathbf{H} = \begin{pmatrix} u\omega \\ v\omega \\ w\omega \end{pmatrix}$$

The first three source terms on the right hand side of equation (2) are contributions from hydrostatic pressure, dynamic pressure and turbulent diffusion, respectively. These terms can be formulated as

$$\mathbf{S}_h = \begin{pmatrix} g\eta\frac{\partial h}{\partial x} \\ g\eta\frac{\partial h}{\partial y} \\ 0 \end{pmatrix} \quad \mathbf{S}_p = \begin{pmatrix} -\frac{D}{\rho_0}(\frac{\partial p}{\partial x} + \frac{\partial p}{\partial \sigma}\frac{\partial \sigma}{\partial x^*}) \\ -\frac{D}{\rho_0}(\frac{\partial p}{\partial y} + \frac{\partial p}{\partial \sigma}\frac{\partial \sigma}{\partial y^*}) \\ -\frac{1}{\rho_0}\frac{\partial p}{\partial \sigma} \end{pmatrix} \quad \mathbf{S}_\tau = \begin{pmatrix} DS_{\tau_x} \\ DS_{\tau_y} \\ DS_{\tau_z} \end{pmatrix}$$

The fourth term is the baroclinic pressure gradient forcing, which is generated by the spatial variation of water density. In the following section, we will show that the suspended sediment may change the density of water-sediment mixture. The last term on the right-hand side of equation (2) accounts for the vegetation-induced drag force and inertia force. For rigid circular cylinders (used in the current study), the vegetation patch can be described by the following parameters: the cylinder diameter d, the number of cylinder per unit area n, the frontal area per unit volume $\lambda = nd$, and the average solid volume fraction of the patch $\phi = n(\pi d^2/4)$. The vegetation patch imposes friction and form drag force on the flow, which are usually modeled together as

$$f_{di} = \frac{1}{2}C_D\lambda u_i|\mathbf{u}| \tag{3}$$

where $\mathbf{u}$ is the velocity vector. C_D is the drag coefficient. For rigid cylinders, the typical value of C_D is 1.0-1.5. For oscillatory flow, inertia force is not negligible and is given by

$$f_{vmi} = C_M\frac{\pi d^2}{4}n\frac{\partial u_i}{\partial t} \tag{4}$$

where C_M is the virtual mass coefficient. Thus, the vegetation-induced source term in equation (2) can be written as

$$\mathbf{S}_{vi} = -D(f_{di} + f_{vmi}) \tag{5}$$

To solve the water depth D, we integrate the continuity equation (1) from $\sigma = 0$ to 1. By using the boundary conditions at the bottom and surface for ω, we may obtain the equation for free surface movement.

$$\frac{\partial D}{\partial t} + \frac{\partial}{\partial x}(D\int_0^1 u d\sigma) + \frac{\partial}{\partial y}(D\int_0^1 v d\sigma) = 0 \tag{6}$$

Sediment Model

The suspended sediment concentration can be computed from the convection-diffusion equation, which is formulated in σ coordinate as follows.

$$\begin{aligned}\frac{\partial DC}{\partial t} + \frac{\partial DuC}{\partial x} + \frac{\partial DvC}{\partial y} + \frac{\partial(\omega - w_s)C}{\partial \sigma} &= \frac{\partial}{\partial x}[D(\nu + \frac{\nu_t}{\sigma_h})\frac{\partial C}{\partial x}] \\ &+ \frac{\partial}{\partial y}[D(\nu + \frac{\nu_t}{\sigma_h})\frac{\partial C}{\partial y}] + \frac{1}{D}\frac{\partial}{\partial \sigma}[(\nu + \frac{\nu_t}{\sigma_v})\frac{\partial C}{\partial \sigma}]\end{aligned} \tag{7}$$

where C is the concentration of suspended sediment and w_s is sediment settling velocity. Note that w_s is not affected by the transformation of coordinates from the Cartesian coordinate system into the σ coordinate system (Wang and Pinardi, 2002). σ_h and σ_v are horizontal and vertical Schmidt numbers for sediment, respectively. To solve the sediment transport equation, no-flux boundary condition is employed at the free surface.

$$(\nu + \frac{\nu_t}{\sigma_v})\frac{1}{D}\frac{\partial C}{\partial \sigma} + w_s C = 0 \tag{8}$$

At the bottom, mass exchange of suspended sediment occurs, resulting in sediment erosion and deposition. This mass exchange can be expresses as the sum of a downward flux $w_s C$ and an upward flux due to various suspension mechanisms, which is usually described by a pickup function.

$$(\nu + \frac{\nu_t}{\sigma_v})\frac{1}{D}\frac{\partial C}{\partial \sigma} = \phi(\theta) \tag{9}$$

In this paper, we adopt the sediment pickup formula suggested by van Rijn (1984).

$$\frac{\phi(\theta)}{\sqrt{(s_s-1)gd}} = 3.3\times10^{-4}\left[\frac{\theta-\theta_c}{\theta_c}\right]^{3/2}\left[\frac{(s_s-1)gd^3}{\nu^2}\right] \tag{10}$$

in which the critical Shields number is $\theta_c = 0.05$. The Shields number θ is related to the bottom shear stress τ_b, which is derived by matching the velocities with the "logarithmic law of the wall".

$$\tau_b = \rho C_f |\mathbf{u_b}|\mathbf{u_b} \tag{11}$$

where $\mathbf{u_b}$ is the current velocity in the first grid point nearest the bottom, C_f is the drag coefficient.

The suspended sediment and flow are simulated in a coupled manner (Ma et al., 2014c). Three effects of suspended sediment on turbulent flow field are considered: (1) baroclinic forcing effect; (2) turbulence damping effect and (3) bottom boundary layer effect. The suspended sediment may change the density of water-sediment mixture, which can be formulated as

$$\rho = (1-C)\rho_0 + C\rho_s \tag{12}$$

where ρ_0 is the reference water density and ρ_s is the sediment density. From the above equation, we see that the spatial variation of suspended sediment concentration can produce the baroclinic pressure gradient forcing $\mathbf{S}_\rho$. In addition, the suspended sediment creates a stably stratified water column, damping fluid turbulence and reducing turbulent diffusivity, which will be considered in the turbulence closure. The suspension of sediment also produces a stably stratified bottom boundary layer. Consequently, the drag coefficient and bottom shear stress are reduced. These effects are accounted for through the modification of bottom boundary condition.

Turbulence Closure

A nonlinear $k-\epsilon$ turbulence model has been implemented into NHWAVE to simulate turbulent flow. In this model, the turbulent eddy viscosity is calculated as

$$\nu_t = C_\mu \frac{k^2}{\epsilon} \tag{13}$$

Within the vegetation patch, mean flow is greatly reduced by the vegetation drag. The large-scale mean kinetic energy is converted to small-scale turbulent kinetic energy (Nepf, 1999). The turbulent diffusivity would also be reduced due to the downward shifting of turbulent length scale (Nepf, 1999). These processes are modeled by introducing vegetation-induced turbulence production terms in the $k-\epsilon$ equations. The turbulence production generated by vegetation is related to the drag force and can be formulated as

$$P_v = u_i f_{di} = \frac{1}{2} C_D \lambda |\mathbf{u}|^3 \tag{14}$$

Thus, the $k-\epsilon$ equations written in conservative forms read

$$\frac{\partial Dk}{\partial t} + \nabla\cdot(D\mathbf{u}k) = \nabla\cdot\left[D\left(\nu + \frac{\nu_t}{\sigma_k}\right)\nabla k\right] + D\left(P_s + P_b + C_{fk}P_v - \epsilon\right) \tag{15}$$

$$\frac{\partial D\epsilon}{\partial t} + \nabla\cdot(D\mathbf{u}\epsilon) = \nabla\cdot\left[D\left(\nu + \frac{\nu_t}{\sigma_\epsilon}\right)\nabla\epsilon\right] + \frac{\epsilon}{k}D\left(C_{1\epsilon}(P_s + C_{3\epsilon}P_b + C_{f\epsilon}P_v) - C_{2\epsilon}\epsilon\right) \tag{16}$$

where $\sigma_k, \sigma_\epsilon, C_{1\epsilon}, C_{2\epsilon}, C_\mu$ are empirical coefficients (Rodi, 1987).

$$\sigma_k = 1.0, \quad \sigma_\epsilon = 1.3, \quad C_{1\epsilon} = 1.44, \quad C_{2\epsilon} = 1.92, \quad C_\mu = 0.09 \tag{17}$$

P_s and P_b are shear and buoyancy productions, which are described as

$$P_s = -\overline{u_i' u_j'}\frac{\partial u_i}{\partial x_j^*} \tag{18}$$

and

$$P_b = \frac{g}{\rho_0}\frac{\nu_t}{D}\frac{\partial \rho}{\partial \sigma} \tag{19}$$

in which the Reynolds stress $\overline{u_i' u_j'}$ is calculated by a nonlinear model proposed by Lin and Liu (1998) for breaking waves, which is given by

$$\begin{aligned}
\overline{u_i' u_j'} = &- C_d \frac{k^2}{\epsilon}\left(\frac{\partial u_i}{\partial x_j^*} + \frac{\partial u_j}{\partial x_i^*}\right) + \frac{2}{3}k\delta_{ij} \\
&- C_1 \frac{k^3}{\epsilon^2}\left(\frac{\partial u_i}{\partial x_l^*}\frac{\partial u_l}{\partial x_j^*} + \frac{\partial u_j}{\partial x_l^*}\frac{\partial u_l}{\partial x_i^*} - \frac{2}{3}\frac{\partial u_l}{\partial x_k^*}\frac{\partial u_k}{\partial x_l^*}\delta_{ij}\right) \\
&- C_2 \frac{k^3}{\epsilon^2}\left(\frac{\partial u_i}{\partial x_k^*}\frac{\partial u_j}{\partial x_k^*} - \frac{1}{3}\frac{\partial u_l}{\partial x_k^*}\frac{\partial u_l}{\partial x_k^*}\delta_{ij}\right) \\
&- C_3 \frac{k^3}{\epsilon^2}\left(\frac{\partial u_k}{\partial x_i^*}\frac{\partial u_k}{\partial x_j^*} - \frac{1}{3}\frac{\partial u_l}{\partial x_k^*}\frac{\partial u_l}{\partial x_k^*}\delta_{ij}\right)
\end{aligned} \tag{20}$$

where C_d, C_1, C_2 and C_3 are empirical coefficients as given by Lin and Liu (1998) as well as Ma et al. (2011).

$$\begin{aligned}
C_d &= \frac{2}{3}\left(\frac{1}{7.4 + 2S_{max}}\right), \quad C_1 = \frac{1}{185.2 + 3D_{max}^2} \\
C_2 &= -\frac{1}{58.5 + 2D_{max}^2}, \quad C_3 = \frac{1}{370.4 + 3D_{max}^2}
\end{aligned} \tag{21}$$

where

$$\begin{aligned}
S_{max} &= \frac{k}{\epsilon} max\left\{\left|\frac{\partial u_i}{\partial x_i^*}\right| \text{(indices not summed)}\right\} \\
D_{max} &= \frac{k}{\epsilon} max\left\{\left|\frac{\partial u_i}{\partial x_j^*}\right|\right\}
\end{aligned} \tag{22}$$

The drag-related coefficients C_{fk} and $C_{f\epsilon}$ in equations (15) and (16) deserve more discussions. Shimizu and Tsujimoto (1994) chose values of $C_{fk} = 0.07$ and $C_{f\epsilon} = 0.16$ based on calibration for the vegetated open channel flow. Lopez and Garcia (1998) discussed them based on a theoretical argument, and suggested that the weighing coefficient C_{fk} should be set to unity if the total turbulence kinetic energy is to be modeled. The coefficient $C_{f\epsilon}$ is related to C_{fk} by $C_{f\epsilon} = C_{2\epsilon}/C_{1\epsilon}C_{fk} = 1.33$. In the following applications, we select the theoretical values suggested by Lopez and Garcia (1998). The coefficient $C_{3\epsilon}$ is chosen to be zero for stably stratified water column (Snyder and Hsu, 2011).

Numerical Schemes and Boundary Conditions

A combined finite-volume and finite-difference scheme with a Godunov-type method is employed to discretize equations (1) and (2) (Ma et al., 2012; Shi et al., 2012). In order to apply Godunov-type scheme, all the variables are defined at the cell centers except that dynamic pressure p is defined at the vertically-facing cell faces. The momentum equations are solved by a second-order Godunov-type finite volume method. The HLL approximate Riemann solver is used to estimate fluxes at the cell faces.

For sediment transport and $k - \epsilon$ equations, the convective fluxes are determined by the hybrid linear/parabolic approximation (HLPA) scheme (Zhu, 1991), which has approximately second-order accuracy in space. Two-stage second-order nonlinear Strong Stability-Preserving (SSP) Runge-Kutta scheme (Gottlieb et al., 2001) was adopted for adaptive time stepping. Uniform gridding is used in the horizontal direction while gridding in the vertical direction is generalized to be non-uniform in order to capture the bottom and surface boundary layers when desired. The Poisson equation for the pressure field, described in Ma et al. (2012), is discretized by the finite-difference method, resulting in an asymmetric coefficient matrix with a total of 15 diagonal lines. The linear system is solved using the high performance preconditioner HYPRE software library. The model is fully parallelized using Message Passing Interface (MPI) with non-blocking communication. Further details of the numerical method may be found in Ma et al. (2012).

To solve the equations, boundary conditions are required for all the physical boundaries. Specifically, at the free surface, we have

$$\frac{\partial u}{\partial \sigma}|_{\sigma=1} = \frac{\partial v}{\partial \sigma}|_{\sigma=1} = 0, \quad w|_{\sigma=1} = \frac{\partial \eta}{\partial t} + u\frac{\partial \eta}{\partial x} + v\frac{\partial \eta}{\partial y} \tag{23}$$

Dynamic pressure is zero at the free surface. For the $k-\epsilon$ model, zero gradients of k and ϵ are imposed.

$$\frac{\partial k}{\partial \sigma}|_{\sigma=1} = \frac{\partial \epsilon}{\partial \sigma}|_{\sigma=1} = 0 \tag{24}$$

At the bottom, the normal velocity and the tangential stress are prescribed. The normal velocity w is imposed through the kinematic boundary condition.

$$w|_{\sigma=0} = -u\frac{\partial h}{\partial x} - v\frac{\partial h}{\partial y} \tag{25}$$

For the horizontal velocities, bottom shear stresses are considered.

$$\nu_t \frac{\partial \mathbf{u}}{\partial \sigma}|_{\sigma=0} = DC_f|\mathbf{u}_b|\mathbf{u}_b \tag{26}$$

where C_f is the bed drag coefficient, which can be specified or computed from the law of the wall for fully rough, turbulent flow. For stably stratified flow, it is formulated as (Wang, 2002)

$$C_f = \left[\frac{1 + AR_f}{\kappa} ln\left(\frac{30\Delta z_1}{k_s}\right)\right]^{-2} \tag{27}$$

where A is the empirical constant (=5.5) (Wang, 2002), R_f is the flux Richardson number, referred to as an index of the vertical density stratification. $\Delta z_1 = 0.5D\Delta\sigma_1$ is the thickness of the cell above the bed, and k_s is the bottom roughness height and $\mathbf{u}_b$ is the velocity at the cell above the bed. The boundary conditions for k and ϵ become

$$k_b = \frac{u_*^2}{\sqrt{C_\mu}} \quad \epsilon_b = \frac{u_*^3}{\kappa z} \tag{28}$$

in which $u_* = \sqrt{C_f}|u_b|$ is the friction velocity.

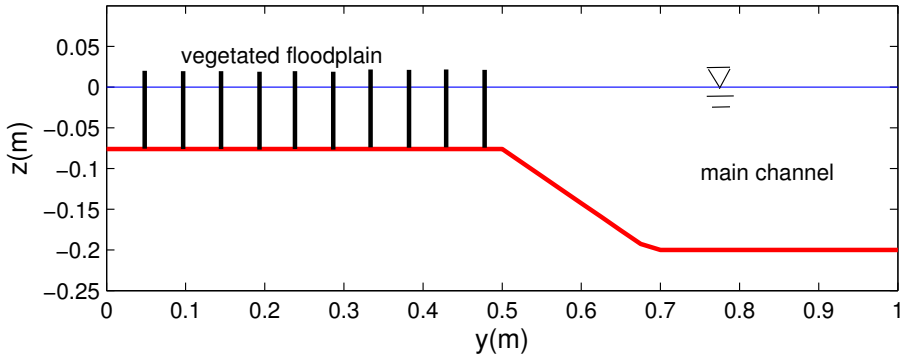

Figure 1: Cross-section geometry and vegetation arrangement in the experiments of Pasche and Rouve (1985). The cross section consists of a main channel and a vegetated floodplain joined by a transition slope.

RESULTS AND DISCUSSIONS

Flow in A Straight Channel with Vegetated Floodplain

The model is firstly validated against laboratory measurements of Pasche and Rouve (1985), who performed a series of experiments in a fixed-bed flume to investigate horizontal velocity distributions in a

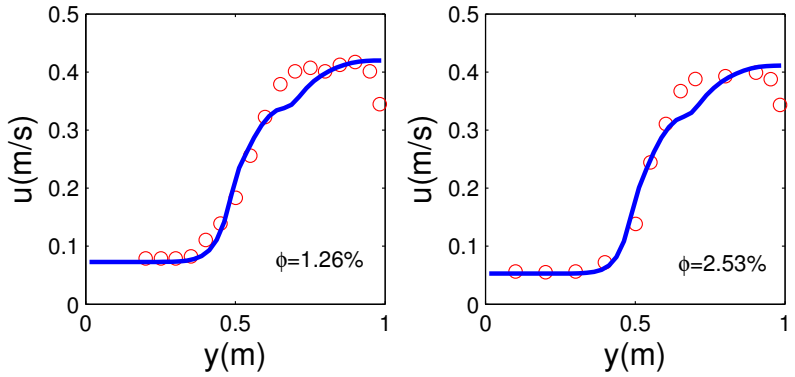

Figure 2: Model-data comparisons of lateral distributions of depth-averaged streamwise flow velocities for two experiments of Pasche and Rouve (1985) with different solid volume ϕ. Lines: simulations; circles: measurements.

compound channel. The channel cross section contained a vegetated floodplain and a main channel joined by a transitional slope (Figure 1). The diameter of the rigid cylinder (modeled vegetation) is d =12 mm. The width of the cross section is 1.0 m. The vegetated floodplain is 0.5 m wide. The bed slope is 0.05%. The flow regime is steady and subcritical with flow rate of 0.0345 m^3/s.

We conducted simulations of two experiments with different vegetation densities n. The corresponding solid volume fractions $\phi = n(\pi d^2/4)$ are 1.26% and 2.53%, respectively. In the simulations, free-slip boundary conditions are imposed at the lateral walls. The vegetation drag coefficient is chosen as the typical value of 1.20. Forty grid cells are employed in the lateral direction to resolve the cross-section distribution of flow velocity. Figure 2 shows the model-data comparisons of lateral distributions of depth-averaged streamwise velocities for two experiments. We see that the simulations agree well with the measurements, except the near-wall regions. The discrepancy is primarily caused by the free-slip boundary conditions we imposed at the lateral walls. At this moment, the model does not have the function to deal with vertical wall boundaries. Away from the walls, the lateral variations of the flow velocity are well captured by the model. Particularly, the model is able to simulate the mean flow reduction induced by vegetation in the floodplain. With increased vegetation density (or solid volume fraction), the mean flow in the floodplain as well as the main channel is reduced.

Nearshore Wave Damping and Sediment Suspension Influenced by A Patch of Vegetation

We will employ the model to examine how vegetation influences nearshore sediment suspension in this section. The computational domain is shown in figure 3(a), which is a wave flume with 12 m long and a beach of 1/20 slope. The bottom is filled with sand of specific gravity $s = 2.65$ and diameter of $d_{50} = 0.15$ mm. The bottom roughness is $k_s = 5.5d_{50} = 0.825$ mm. The domain is discretized by 800 grid cells with grid size of $\Delta x = 0.015$ m. 50 layers with uniform grid size are used in the vertical direction. The incident wave height is $H = 9.9$ cm, wave period is $T = 1.35$ s. The water depth in the flat bottom is $h = 39.5$ cm. The model setup is similar to the laboratory experiment of Sato et al. (1990). We conducted two numerical experiments: one with a patch of vegetation covering the beach from $x = 8$ m to $x = 10$ m, and the other without vegetation. The vegetation density λ is 30 m^{-1}. The vegetative drag coefficient C_D is taken as 0.5, which represents the upper range of values seen for the similarly scaled experimental data (Dubi and Torum, 1997).

Figure 3(a) shows the simulated instantaneous surface elevation with the vegetation patch, from which we can clearly see the attenuation of waves inside the vegetation patch. The direct comparison of wave heights with and without vegetation patch is given in figure 3(b). Similar to the findings of Ma et al. (2014c), the wave height is greatly reduced by the patch. Consequently, the cross-shore gradient of wave height in the offshore part of the patch is greater than that without vegetation, possibly resulting in an increase of wave setup. In the onshore part of the patch, the cross-shore gradient of wave height is smaller than that without vegetation, which would produce a smaller wave setup. From the wave height distribution, it is noticed that the wave breaking happens around $x_b = 8.0$ m, indicating that the vegetation patch is located

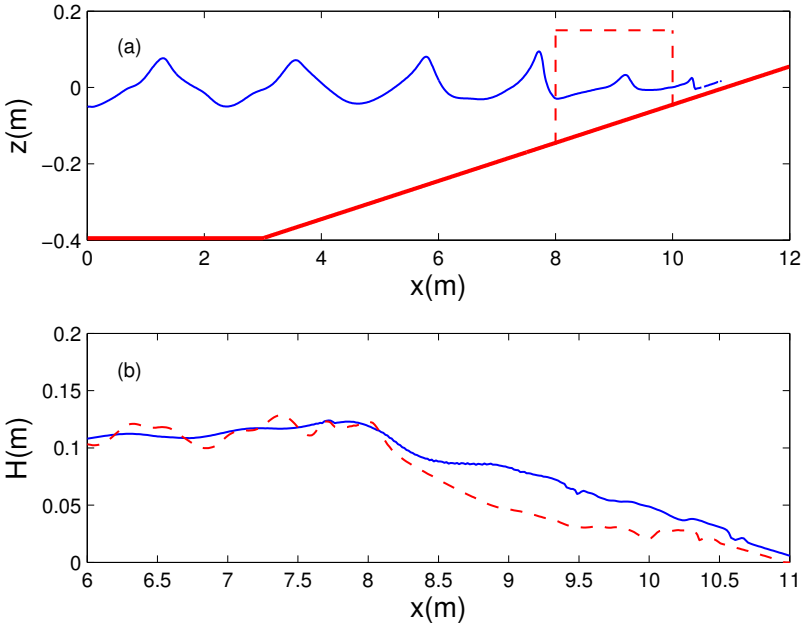

Figure 3: (a) Model setup and simulated instantaneous free surface with vegetation. The patch of the emergent vegetation covers the region from $x = 8$ m to $x = 10$ m. (b) Comparison of simulated cross-shore distributions of wave height with (dashed line) and without (solid line) vegetation patch.

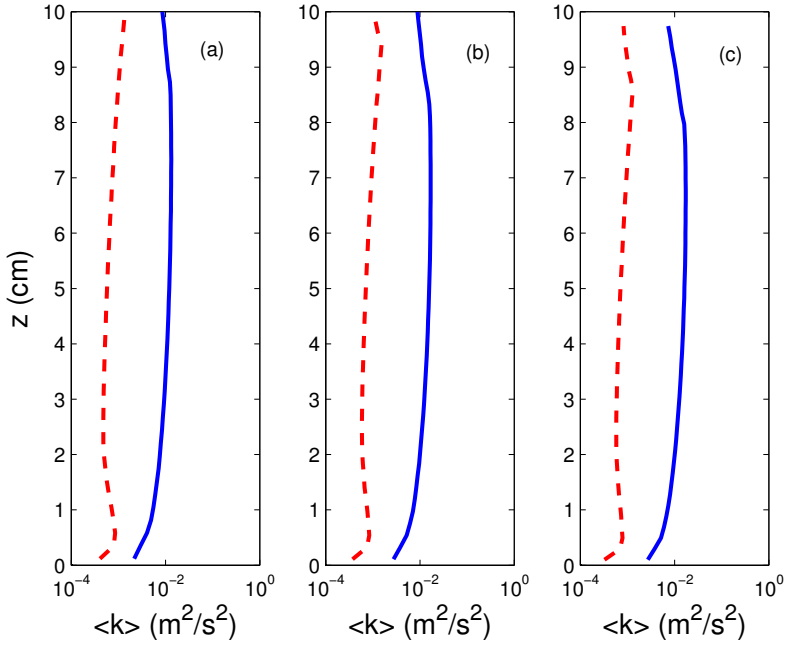

Figure 4: Comparisons of vertical profiles of wave-averaged turbulent kinetic energy with (dashed lines) and without (solid lines) vegetation patch at three stations. (a) $x - x_b = 0.378$ m; (b) $x - x_b = 0.540$ m and (c) $x - x_b = 0.729$ m. x_b is the location of breaking point.

inside the surf zone.

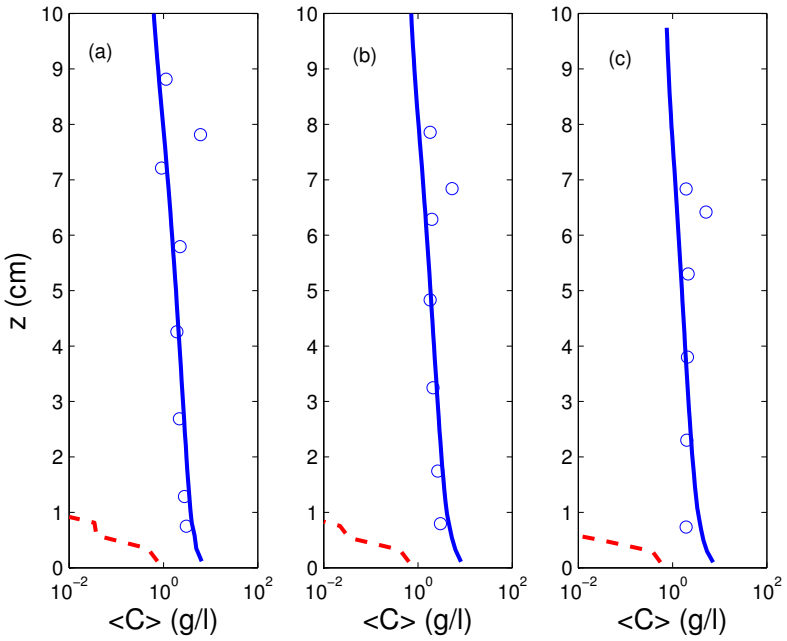

Figure 5: Comparisons of vertical profiles of wave-averaged suspended sediment concentration with (dashed lines) and without (solid lines) vegetation patch at three stations. (a) $x - x_b = 0.378$ **m; (b)** $x - x_b = 0.540$ **m and (c)** $x - x_b = 0.729$ **m.** x_b **is the location of breaking point. Circles represent laboratory measurements.**

Figure 4 compares the predicted wave-averaged turbulent kinetic energy with and without vegetation patch at three stations in the surf zone. It has been widely recognized that the vegetation canopy can greatly reduce mean flow through enhancing resistance to the flow field, consequently compressing turbulence level (Nepf, 1999). In the surf zone, wave breaking generated turbulence is generally intense. However, the vegetation patch can dramatically damp turbulence, resulting in the turbulent kinetic energy (TKE) at least one order of magnitude smaller than that in the unvegetated surf zone as seen in figure 4. It seems that the wave breaking is completely inhibited by the vegetation canopy. The damping of turbulence within the patch would directly affect sediment suspension from the bottom as displayed in figure 5, which compares the vertical profiles of wave-averaged suspended sediment concentration with and without vegetation patch at three stations in the surf zone. To show the model's capability, we also compare the numerical results with laboratory measurements of Sato et al. (1990) in the case of no vegetation patch. In this simulation, the vertical Schmidt number for sediment σ_v is taken as 0.5. We can see that the simulated vertical profiles of wave-averaged suspended sediment concentration agree well with the measurements, indicating that the model is capable of capturing nearshore sediment suspension. With the vegetation patch, the wave-averaged suspended sediment concentration is considerably smaller, indicating that much less sediments are picked up from the bottom. Most of these sediments are restricted in the bottom boundary layer with the thickness of about 1 cm.

The cross-shore sediment fluxes with and without vegetation are examined in figure 6. Following Henderson et al. (2004), we present three sediment fluxes: the mean Eulerian sediment flux $< uC >$, the "current-generated" flux $< u >< C >$ and the "wave-generated" flux $< (u - < u >)(C - < C >) >$. Clearly, the former one equals the sum of the latter two fluxes. Similar to the findings in Ma et al. (2013b), in the surf zone without vegetation, the mean Eulerian sediment flux is seaward, which is contributed by both the "current-generated" flux and "wave-generated" flux. This is due to the strong return flow (undertow) in the surf zone, which generates offshore sediment flux. With the vegetation patch, suspended sediments are mostly restricted in the bottom boundary layer (figure 5). The sediment fluxes are also limited in a thin layer near the bottom. Because wave breaking is inhibited by the vegetation canopy, the undertow is relatively

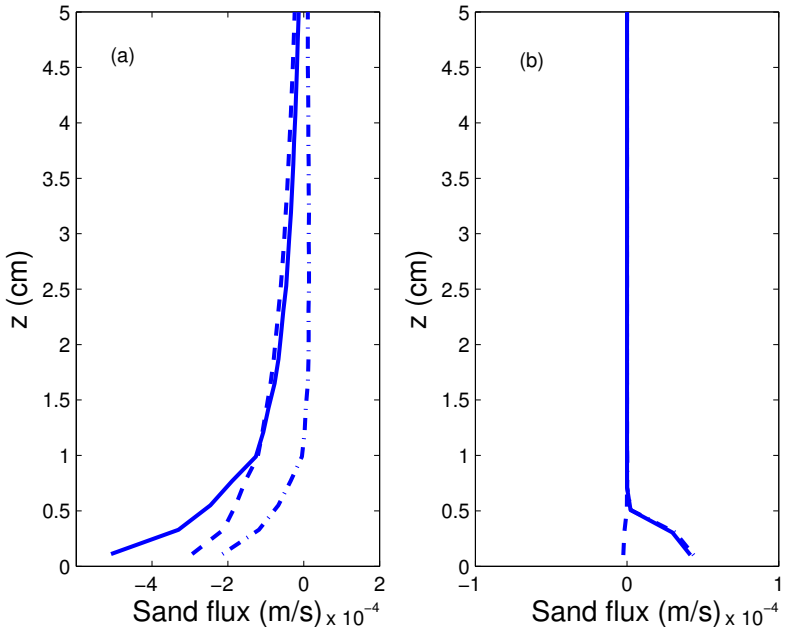

Figure 6: Cross-shore volumetric sediment flux (a) without vegetation and (b) with vegetation at station $x - x_b = 0.729$ m. Solid lines: Eulerian mean sediment flux; dashed lines: mean current-induced sediment flux; dash-dotted lines: wave-induced sediment flux

weak. Therefore, the offshore-directed “current-generated" flux is small. The mean Eulerian sediment flux is shoreward, which is mostly contributed by the “wave-generated" flux due to the skewness and asymmetry of the waves. These sediment fluxes are very similar to that outside the surf zone (Ma et al., 2014c).The shoreward Eulerian sediment flux indicates onshore net sediment transport within the vegetation patch.

CONCLUSIONS

In this paper, we have developed a three-dimensional hydrodynamic and sediment transport for studying flow/wave-vegetation-sediment interactions. The vegetation effects on the mean flow and turbulence were accounted for by introducing additional formulations for drag and turbulence production induced by vegetation canopy. The suspended sediment concentration was obtained by solving the advection-diffusion equation with sediment exchange at the bed. The turbulent flow and suspended sediment are simulated in a coupled manner by considering sediment-induced stratification. The model was validated by the laboratory measurements of partially vegetated open channel flows of Pasche and Rouve (1985). Numerical results showed that the model is capable of simulating vegetated open channel flow.

The model was then applied to study nearshore sediment suspension influenced by a patch of vegetation. It was found that the vegetation canopy could dramatically damp turbulence in the surf zone, resulting in considerably less sediment suspension. Within the vegetation patch, most suspended sediment are restricted in the wave boundary layer. The net sediment transport is shoreward, in contrast to the seaward net sediment transport in the unvegetated surf zone. This shoreward net sediment flux is mostly contributed by the wave-generated flux due to the skewness and asymmetry of the waves.

ACKNOWLEDGEMENTS

The author acknowledges the financial support of Old Dominion University Research Foundation (Multidisciplinary Seed Funding (MSF) Grants, Project No. 545411).

REFERENCES

Abt S., Clary W., Thornton C., 1994, Sediment deposition and entrapment in vegetated streambeds,*J. Irrig. Drain. Eng.* 120, 1098Ð1110

Chen S.-N., Sanford L.P., Koch E.W., Shi F. and North E.W., 2007, A nearshore model to investigate the effects of seagrass bed geometry on wave attenuation and suspended sediment transport, *Estuaries and Coasts*, 30, 296-310

Dubi A. and Torum A., 1995, Wave damping by kelp vegetation. In edge B.L. (Ed.), *Proc. 24th Coast. Eng. Conf.*, ASCE, New York, 142-156

Elliott A. H., 2000, Settling of fine sediment in a channel with emergent vegetation, *J. Hydraulic Eng.*, 126, 570-577

Gacia E., Granata T.C. and Duarte C.M., 1999, An approach to measurement of particle flux and sediment retention within seagrass (Posidonia oceanica) meadows, *Aquatic Botany*, 65, 255Ð268

Gottlieb S., Shu C.-W. and Tadmor E., 2001, Strong stability-preserving high-order time discretization methods, *SIAM Review*, 43, 89-112

Henderson S.M., Allen J.S. and Newberger P.A., 2004, Nearshore sandbar migration predicted by an eddy-diffusive boundary layer model, *J. Geophys. Res.*, 109, C06024, doi:10.1029/2003JC002137

Lin P. and Liu P.L.-F., 1998, A numerical study of breaking waves in the surf zone, *J. Fluid Mech.*, 359, 239-264

Lopez F. and Garcia M., 1998, Open-channel flow through simulated vegetation: Suspended sediment transport modeling, *Water Res. Res.*, 34 (9), 2341-2352

Ma G., Shi F. and Kirby J.T., 2011, A polydisperse two-fluid model for surf zone bubble simulation, *J. Geophys. Res.*, 116, C05010, doi:10.1029/2010JC006667

Ma G., Shi F. and Kirby J.T., 2012, Shock-capturing non-hydrostatic model for fully dispersive surface wave processes, *Ocean Modell.*, 43-44, 22-35

Ma G., Kirby J.T., Su S.-F., Figlus J. and Shi F., 2013a, Numerical study of turbulence and wave damping induced by vegetation canopies, *Coastal Eng.*, 80, 68-78

Ma G., Kirby J.T. and Shi F., 2013b, Numerical simulation of tsunami waves generated by deformable submarine landslides, *Ocean Modell.*, 69, 146-165

Ma G., Su S.-F., Liu S. and Chu J.-C., 2014a, Numerical simulation of infragravity waves in fringing reefs using a shock-capturing non-hydrostatic model, *Ocean Eng.*, 85, 54-64

Ma G., Shi F., Hsiao S.-C. and Wu Y.-T., 2014b, Non-hydrostatic modeling of wave interactions with porous structures, *Coastal Eng.*, 91, 84-98

Ma G., Chou Y.-J. and Shi F., 2014c, A wave-resolving model for nearshore suspended sediment transport, *Ocean Modell.*, 77, 33-49

Nepf H.M., 1999, Drag, turbulence, and diffusion in flow through emergent vegetation, *Water Res. Res.*, 35 (2), 479-489

Pasche E. and Rouve G., 1985, Overbank flow with vegetatively roughened flood plains, *J. Hydraul. Eng.*, 111, 1262-1278

Rodi W., 1987, Examples of calculation methods for flow and mixing in stratified flows, *J. Geophys. Res.*, 92(5), 5305-5328

Sato S., Homma K. and Shibayama T., 1990, Laboratory study on sand suspension due to breaking waves, *Coastal Eng. Jpn.*, 33, 219-231

Sheng Y.P., Lapetina A. and Ma G., 2012, The reduction of storm surge by vegetation canopies: Three-dimensional simulations, *Geophys. Res. Let.*, 39, L20601, doi:10.1029/2012GL053577

Shi F., Ma G., Kirby J.T. and Hsu T.-J., 2012, Application of a TVD solver in a suite of coastal engineering models, *Proc. 33rd Coast. Eng. Conf.*, ICCE2012, Santander, Spain, July 1-6

Shimizu Y. and Tsujimoto T., 1994, Numerical analysis of turbulent open-channel flow over a vegetation layer using a $k-\epsilon$ turbulence model, *J. Hydrosci. Hydraul. Eng.*, 11 (2), 57-67

Sharp R.G. and James C.S., 2006, Deposition of sediment from suspension in emergent vegetation, *Water SA*, 32, 211-218

Snyder P.J. and Hsu T.-J., 2011, A numerical investigation of convective sedimentation, *J. Geophys. Res.*, 116, C09024, doi:10.1029/2010JC006792

Temmerman S., Bouma T.J., Govers G., Wang Z.B., De Vries M.B. and Herman P.M.J., 2005, Impact of vegetation on flow routing and sedimentation patterns: Three-dimensional modeling for a tidal marsh, *J. Geophys. Res.*, 110, F04019, doi:10.1029/2005JF000301

Thornton C. I., Abt S. R., and Clary W. R., 1997, Vegetation influence on small stream siltation, *Journal of The American Water Resource Association*, 33, 1279Ð1288

van Rijn L.C., 1984, Sediment pick-up function, *J. Hydraul. Eng.*, 110,1494-1502

Wang X.H., 2002, Tide-induced sediment resuspension and the bottom boundary layer in an idealized estuary with a muddy bed, *J. Phys. Oceanogr.*, 32(11), 3113-3131

Wang X.H. and Pinardi N., 2002, Modeling the dynamics of sediment transport and resuspension in the Northern Adriatic Sea, *J. Geophys. Res.*, 107(C12), 3225, doi:10.1029/2001JC001303

Wu W., Shields D. Jr., Bennett S.J. and Wang S.S.Y., 2005, A depth-averaged two-dimensional model for flow, sediment transport, and bed topography in curved channels with riparian vegetation, *Water Res. Res.*, 41, W03015, doi:10.1029/2004WR003730

Zhu J., 1991, A low-diffusive and oscillation-free convection scheme, *Comm. Appl. Num. Meth.*, 7, 225-232

Zong L. and Nepf H., 2010, Flow and deposition in and around a finite patch of vegetation, *Geomorphology*, 116, 363-372

Zong L. and Nepf H., 2011, Spatial distribution of deposition with a patch of vegetation, *Water Res. Res.*, 47, W03516, doi:10.1029/2010WR009516